

PCCP

Accepted Manuscript



This is an *Accepted Manuscript*, which has been through the Royal Society of Chemistry peer review process and has been accepted for publication.

Accepted Manuscripts are published online shortly after acceptance, before technical editing, formatting and proof reading. Using this free service, authors can make their results available to the community, in citable form, before we publish the edited article. We will replace this *Accepted Manuscript* with the edited and formatted *Advance Article* as soon as it is available.

You can find more information about *Accepted Manuscripts* in the [Information for Authors](#).

Please note that technical editing may introduce minor changes to the text and/or graphics, which may alter content. The journal's standard [Terms & Conditions](#) and the [Ethical guidelines](#) still apply. In no event shall the Royal Society of Chemistry be held responsible for any errors or omissions in this *Accepted Manuscript* or any consequences arising from the use of any information it contains.

Effects of various kinetic rates of FtsZ filaments on bacterial cytokinesis

Zi He,¹ Zhuan Liu,¹ Kunkun Guo*,¹ and Lina Ding²

¹*College of Materials Science and Engineering,
Hunan University, Changsha, 410082, China*

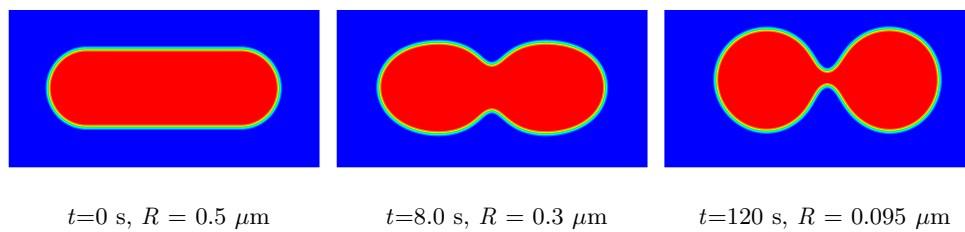
²*School of Pharmaceutical Sciences, Zhengzhou University,
100 Kexue Avenue, Zhengzhou, Henan 450001, China*

(Dated: November 4, 2015)

Cell morphodynamics during bacterial cytokinesis are theoretically explored by a combination of phase field model for rod-shaped cells and a kinetic description for FtsZ ring maintenance. The division times and cell shapes **have been** generally decided by the competition between the constriction forces generated by FtsZ rings and the curvature elastic energy for cells. The dependences of cell morphodynamics during bacterial cytokinesis on various kinetic rates of FtsZ filaments, are focused **in the present study**. It is found that **the obtained results with the experimental parameters are well** comparable to the observed results physiologically. Likewise, the quasi-steady states for FtsZ rings are found to be well consistent with the theoretical results derived from the kinetic description of FtsZ rings. In addition, morphological phase diagram is presented as functions of the membrane associate rate for both short FtsZ filaments and free FtsZ monomers, and the depolymerization rate of GDP-bound FtsZ monomers at the tip of filaments within the ring. **Our results would provide a better understanding of the details of *in vivo* kinetics, including the kinetic rates within FtsZ rings.**

* To whom correspondence should be addressed. Email:kunkunguo@hnu.edu.cn

Cell morphodynamics during bacterial cytokinesis is extensively investigated by a combination of phase field model for rod-shaped cells and a kinetic description for FtsZ ring maintenance.



I. INTRODUCTION

In bacterial cells, filamentous temperature sensitive protein Z (FtsZ), a guanosine triphosphatase (GTPase), is the first protein to localize in the midcell at the division sites as part of the cytokinesis machinery¹. FtsZ proteins assemble into the curved living polymers with a ring-like structure called the FtsZ ring or Z ring under the cytoplasmic membrane¹⁻⁴. In general, the FtsZ ring *in vivo* consists of short polymerized FtsZ filaments **which are** aligned in the circumferential orientation of bacterial cells. However, the complete role of the FtsZ ring in bacterial cytokinesis is still unclear. The FtsZ ring could recruit other cell division factors, **as well as** provide the force required to constrict the membrane by guanosine triphosphate (GTP) hydrolysis^{2,5}. Without GTP hydrolysis or with the replacement of GTP with a slowly hydrolysable GTP analogue (GMPCPP), FtsZ ring can still form and generate an initial constriction force⁶⁻⁸. However, the constriction would quickly stop because FtsZ rings become rigidly stabilized in the absence of GTP hydrolysis.

Proper localization of the FtsZ ring to the midcell is accomplished by at least two mechanisms **that are** nucleoid occlusion and inhibition of polar FtsZ assembly by the Min system^{2,9,10}. The Min system involves proteins MinC, MinD, and MinE^{1,11,12}. MinC protein inhibits the assembly of the FtsZ ring by increasing the depolymerization rate of GDP-bound FtsZ monomers within filaments, **or** by reducing the associated rate of FtsZ monomers to filaments, **even** by occupying binding sites on the FtsZ filament lattice. While, the MinD and MinE proteins serve to exclude the MinC proteins from the midcell region, promoting the assembly of the FtsZ ring at the midcell. In addition to the Min proteins, a diverse array of other regulatory proteins have been identified during the FtsZ assembly, broadly classifying into negative and positive¹³. Negative factors, that is, FtsZ inhibitors, prevent the FtsZ ring polymerized at the poles or over the nucleoid. **These negative factors could play** a critical role in ensuring the dynamics of the FtsZ ring at the future division site¹⁴. For example, EzrA and SulA (negative factors) interact either with FtsZ or with one of its binding partners to promote depolymerization. Positive factors, known as FtsZ stabilizers, such as ZapA proteins, can promote the assembly and maturation of a stable FtsZ ring. In general, positive factors are required to nucleate, tether, and/or stabilize FtsZ polymers at the site of future division¹⁵.

Previous studies of the nucleotide-dependent bending of FtsZ filaments present that either straight or gently curved filaments are assembled by purified FtsZ proteins with a radius of curvature of approximately 100 nm in the presence of GTP, while highly curved filaments are formed with a curvature radius of approximately 10 nm in the presence of GDP^{6,16-19}. Rapid transformation transitions between straight and curved FtsZ filaments during GTP hydrolysis cycles are observed experimentally, and could generate the mechanical forces larger than 8 pN that is the amount of force required for cell wall invagination during bacterial cytokinesis²⁰. In addition, the regulators of FtsZ polymerization bound to FtsZ monomers, are expected to influence the mechanical properties of FtsZ protofilaments by their incorporations into the FtsZ ring or by causing the transitions of dominant FtsZ proteins between native structures. These would provide mechanisms for the cell cycle regulatory network to control the intrinsic curvature parameters of the FtsZ ring^{2,9,10}.

It is still unclear that how the constriction force is generated by FtsZ ring and how FtsZ ring plays an important role in the cell division²¹. One mechanism for the force generation of the FtsZ ring has been proposed that the couple of GTP hydrolysis causes the transitions between straight and highly curved conformation of FtsZ protofilaments, thereby generating the bending force^{6,16-18}. The other mechanism is that the cooperativity of the polymerization, the condensation and bundling of FtsZ filaments are revealed, thereby leading to the constriction of the FtsZ ring and the decrease of the circumference²²⁻²⁴. One theoretical framework²⁷ has been recently developed to couple cell shapes with FtsZ rings system, which combines a kinetic description of FtsZ-ring maintenance^{25,27} with phase field dynamics for cell morphodynamics^{26,28}. Phase field model²⁹⁻³² has been widely used to study vesicle dynamics and cell morphodynamics. While, the kinetic description in our study includes the incorporation of short filaments and free FtsZ monomers into the ring, GTP hydrolysis within the ring and rapidly nucleotide exchange in the cytoplasmic pool, and disassembly of both GTP-bound and GDP-bound monomers at the tips of the filament in the ring, the mechanical characterization of both GTP-bound and GDP-bound monomers within FtsZ rings²⁷. This theoretical framework has been successfully applied to study the dynamic process of cell constrictions, as well as cell morphodynamics as functions of various initial states of rod-shaped cells and FtsZ rings²⁷. Herein, this theoretical framework is extended to discuss the dependences of various kinetic rates on cell morphodynamics during bacterial cytokinesis.

This paper is organized as follows. Section II describes the theoretical framework by a combination of phase field model for cells and the kinetic model for FtsZ-ring turnover, and the numerical calculation method. In section III, cell morphodynamics during bacterial cytokinesis are discussed as functions of the membrane associate rate, the depolymerization rates of GTP-bound and GDP-bound FtsZ monomers at the tips, GTP hydrolysis rate, and the intrinsic curvature of GTP-bound and GDP-bound FtsZ monomers within the ring. Phase diagram is also presented as functions of the membrane associate rate and the depolymerization rate of GDP-bound FtsZ monomers. Finally, section IV contains a brief summary and outlook.

II. THEORETICAL METHOD

The study is motivated by the experimental observations of cell division for *E. Coli* in the presence of FtsZ ring. The kinetic rates, such as the depolymerization rates of FtsZ monomers at the tips of filaments, the membrane associate rates and intrinsic curvature of FtsZ monomers within the ring, can be changed in the presence of various regulatory proteins. As expected, these kinetic rates of FtsZ filaments would affect the dynamic turnover of the FtsZ ring, thereby leading to the **changes** of cell constrictions. In the previous study²⁷, we have developed one computational model by a combination of phase field model for cells and a kinetic description for dynamic turnover of FtsZ rings, to study the dynamic processes of cell constrictions and changes of constrictive forces upon different initial states of rod-shaped cells and FtsZ rings.

The theoretical framework has been thoroughly presented in the previous study²⁷. It starts that the assumption of typical bacteria, **such as *E. Coli* and *B. subtilis***, takes approximately as a two-dimensional rod-shaped cell with a fixed A_0 , see Fig. 1. **The dynamic turnover of short FtsZ filaments is considered to be coupled with GTP hydrolysis.** The FtsZ ring consisting of several short FtsZ filaments is generally located in the midcell, as shown in Fig. 1 (b). An auxiliary phase field, ϕ , is introduced to distinguish the interior or exterior of the cell, taking 1 in the interior of the cell wall but $\phi = 0$ in the cell exterior. This field changes abruptly between the diffusive interface with two limited values, $\phi = 1$ and $\phi = 0$. The width of cell wall/membrane is approximately equal to this interface, ϵ .

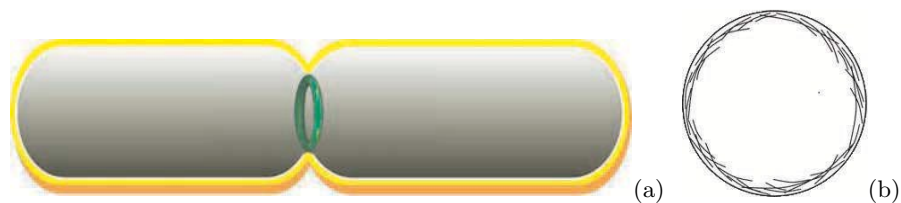


FIG. 1. (color online) (a) A rod-shaped cell with FtsZ ring distributed in the middle of cell along the horizontal direction is schematically illustrated, where the the diffusion interface with a width of ϵ is indicated by yellow color, the interior of the cell, $\phi = 1$ is grey color, while the cell exterior with $\phi = 0$ is white color, and FtsZ ring is green and located in the middle of rod-shaped cell. (b) Enlarged view of the FtsZ ring in midcell consisting of short FtsZ filaments.

The dynamic evolution equation for the phase field referred by previous studies^{26,29,30} is given by

$$\frac{\partial \phi}{\partial t} = -\mathbf{u} \cdot \nabla \phi + \Gamma [\epsilon \nabla^2 \phi - \frac{G'}{\epsilon} + \epsilon c |\nabla \phi|] \quad (1)$$

where the advection term presents that the phase field is coupled by the local flow velocity, \mathbf{u} , the parameter ϵ is the width of the cell wall, Γ is **non-negative mobility efficient (its magnitude with respect to ϵ)**, the local curvature c is equal to $-\nabla \cdot \frac{\nabla \phi}{|\nabla \phi|}$, and a double well potential, G , is $18\phi^2(1 - \phi^2)$ with **two minima** at $\phi = 1$ and $\phi = 0$. The last term of the right side of the equation, similar to previous works^{29,30}, is introduced to stabilize the phase field interface, as well as cancel surface-like energy which is not desirable for vesicles.

As previously presented²⁷, cell constrictions in the presence of FtsZ ring are determined by the interactions of various forces, including the surface tension, the bending force, the pressure that constrains the cell area of vesicles, as can be volume in three dimensions, the radial and contraction force generated from FtsZ rings in the midcell, and the effective friction due to cell divisions and cell motile. In addition, the perimeter of the cell wall, as can be surface area in three dimensions, is not fixed because proteins or lipid molecules can enter into or escape from cell membrane during the biological processes such as cell wall expansions and cell divisions. Firstly, the surface energy can be implemented in the phase-field formulations as^{31,32}

$$H_{te} = \gamma L = \gamma \int (\frac{\epsilon}{2} |\nabla \phi|^2 + \frac{G}{\epsilon}) d\mathbf{r} \quad (2)$$

and is proportional to the cell's perimeter L , where γ is the surface tension. By the derivation of the surface

energy, the area density of surface tension force is given by

$$\mathbf{F}'_{te} = -\frac{\delta H_{te}}{\delta \mathbf{R}} = \frac{\delta H_{te}}{\delta \phi} \nabla \phi = -\gamma(\epsilon \nabla^2 \phi - \frac{G'}{\epsilon}) \nabla \phi. \quad (3)$$

Due to the study in two dimensions, this area density has to be converted into a line density using $\mathbf{F}'_{te} d\mathbf{r} = \mathbf{F}_{te} \epsilon |\nabla \phi|^2 d\mathbf{r}^{26}$. Therefore, the surface tension force with a line density is

$$\mathbf{F}_{te} = -\gamma(\nabla^2 \phi - \frac{G'}{\epsilon^2}) \frac{\nabla \phi}{|\nabla \phi|^2} \quad (4)$$

The bending energy H_{be} of the cell wall is given as follows^{31,32}

$$H_{be} = \frac{\kappa}{2} \int \frac{1}{\epsilon} [\epsilon \nabla^2 \phi - \frac{G'}{\epsilon}]^2 d\mathbf{r} \quad (5)$$

where κ is the bending rigidity of the cell wall. The spontaneous curvature is assumed to be zero. The area density of the bending force can be derived, and **also be converted into a line density as mentioned above**. The bending force with a line density is given as follows²⁶

$$\mathbf{F}_{be} = \kappa(\nabla^2 - \frac{G''}{\epsilon^2})(\nabla^2 \phi - \frac{G'}{\epsilon^2}) \frac{\nabla \phi}{|\nabla \phi|^2}. \quad (6)$$

Cell area in two dimensions, which is equivalent to volume in three dimensions, $A = \int \phi d\mathbf{r}$ is observed to be conserved during cell divisions in the experiment³³, but the perimeter is not highly conserved. Therefore, a constraint term is introduced to guarantee the cell area with the phase field formulation of

$$H_{ar} = -\frac{M_A}{2} (A(\phi) - A_0)^2 \quad (7)$$

where M_A is large and A_0 is the prescribed area. The force is given by the derivation of the constraint term

$$\mathbf{F}_{ar} = M_A (\int \phi d\mathbf{r} - A_0) \frac{\nabla \phi}{|\nabla \phi|}. \quad (8)$$

As previously presented, FtsZ rings provide a retraction force to the cell wall/membrane, thereby leading to cell divisions. A stable and smooth FtsZ ring is assumed to form in the midcell, leading to the homogeneous distribution of hydrolyzed and unhydrolyzed monomers and the uniform effect on the cell membrane or cell wall. Therefore, a mechanical averaging across the thickness of the ring is reasonable justified, as well as the

linear elasticity is desirable for the FtsZ ring. Thus, the mechanical energy H_z stored in the FtsZ ring as functions of its radius and FtsZ monomers is given by³⁴

$$H_z = \frac{1}{2} \int B \left(\kappa(s) - \frac{1}{R} \right)^2 ds = \frac{B\delta}{2} \left((S - S_D) \left(\kappa_T - \frac{1}{R} \right)^2 + S_D \left(\kappa_D - \frac{1}{R} \right)^2 \right) \quad (9)$$

where B is the bending modulus of a FtsZ filament. $\kappa(s)$ is the preferred curvature as a function of position in the ring (s), **and the value of κ is equal to either κ_T or κ_D which depends on its hydrolysis state of the ring at that position (GTP- or GDP-bound respectively).** δ is the size of a monomer and R is the radius of the ring. The total number of FtsZ monomers and the GDP-bound FtsZ monomers in the ring are S and S_D , respectively. The radial force generated by the ring is given by the derivation of mechanical energy H_z with respect to radius R ,

$$\mathbf{F}_z = - \frac{\delta H_z}{\delta R} \cdot \mathbf{n} = \frac{B\delta S}{R^3} \left(R\kappa_T - 1 - \frac{S_D}{S} (\kappa_T - \kappa_D) R \right) \frac{\nabla\phi}{|\nabla\phi|} \quad (10)$$

where \mathbf{n} denotes the generated force along the normal direction to the cell wall.

Prior to achieve the mechanical energy H_z of the FtsZ-ring given by the equation (9), the total number of FtsZ monomers and GDP-bound FtsZ monomers within the ring have to be obtained. In our theoretical framework as presented in Ref. 27, the kinetic description of the FtsZ ring turnover includes the incorporation of new short filaments and free FtsZ monomers into the ring, the hydrolysis of GTP-bound monomers within the ring, and the disassembly of both GTP-bound and GDP-bound monomers from the ring, as well as the mechanical characterization of both GTP-bound and GDP-bound monomers in the FtsZ-ring used for the analysis of force generation. Two main physical quantities are introduced that are the length distribution of filaments in the ring, $p(l, t)$, and the number of hydrolyzed monomers, $S_D(t)$ within the ring, where l is the number of monomers in the filament at time t . Other quantities of the total number of FtsZ monomers, S , and filament tips, F , within the ring can be subsequently obtained from $S = \int_0^\infty lp(l, t)dl$ and $F = \int_0^\infty p(l, t)dl$, respectively. The cytosolic concentration of FtsZ monomers obeys with the relation of $Z_T - S/(N_cA)$, where Z_T is the total concentration of FtsZ monomers in the cell, and the factor N_cA is employed to transform the number of molecules to concentration in micromoles.

The length of cytosolic filaments is generally assumed to obey a quasi-steady exponential distribution with a mean length λ , similar to the experimental observation¹³. The incorporation rate of filaments with a length

of l is proportional to the cytosolic concentration of those filaments. The incorporated filaments **generally** contain some fraction of hydrolyzed monomers, **but** the assumption that the cytosolic filaments consist entirely of GTP-bound FtsZ monomers is reasonable²⁵. **Likewise**, the depolymerization of monomers is governed by not only its position within a filament but also the nucleotide state³⁵. The depolymerization rates of GTP-bound and GDP-bound FtsZ monomers at the filament tips are defined as κ_{off}^T and κ_{off}^D , respectively. The fractions of GDP-bound and GTP-bound monomers are expressed in the form of $f_D = S_D/S$ and $1 - S_D/S = 1 - f_D$, respectively.

The assumption of filaments is randomly distributed throughout the ring. The filament length distribution $p(l, t)$ is accomplished with both the incorporation of FtsZ filaments/free FtsZ monomers from the cytosol and the depolymerization of monomers from filament tips. Therefore, the filament length distribution $p(l, t)$ within the ring obeys with **the evolution equation of**²⁵

$$\frac{\partial p(l, t)}{\partial t} = 4\pi R \kappa_{\text{in}} \left(Z_T - \frac{S}{N_c A} \right) \frac{1}{\lambda} \exp(-l/\lambda) + [\kappa_{\text{off}}^T \left(\frac{S - S_D}{S} \right) + \kappa_{\text{off}}^D \left(\frac{S_D}{S} \right)] [p(l+1, t) - p(l, t)] \quad (11)$$

where κ_{in} is the membrane associate rate, and $4\pi R$ accounts for the number of available binding sites for new filaments, because the binding sites are assumed only to associate along the outer edges of the barrel-shaped FtsZ ring.

The number of GDP-bound FtsZ monomers within the ring, S_D , relevant to both GTP hydrolysis and the depolymerization of GDP-bound FtsZ monomers at the tips, evolves as follows

$$\frac{\partial S_D}{\partial t} = \kappa_{\text{hy}}(S - S_D) - \kappa_{\text{off}}^D \frac{S_D}{S} F \quad (12)$$

The first term accounts for GTP hydrolysis that GTP-bound monomers within the FtsZ ring can hydrolyze in a stochastic manner independent of the state of adjacent monomers, and the second term accounts for the depolymerization of GDP-bound monomers at all filament tips within the ring F . **Integrating the length distribution of filaments in the ring, the total number of filament tips, F , is deduced.** The rate of GTP-bound monomers hydrolyzed into GDP-bound ones **is defined as** κ_{hy} . By combining Eq. (11) and (12), the quasi-steady state for this subsystem **is given as follows**

$$S_{\text{qss}} = \frac{4\pi R N_c A Z_T \kappa_{\text{in}} \lambda^2 (\kappa_{\text{off}}^D + \kappa_{\text{hy}} \lambda)}{4\pi R \lambda^2 \kappa_{\text{in}} (\kappa_{\text{off}}^D + \kappa_{\text{hy}} \lambda) + \kappa_{\text{off}}^D N_c A (\kappa_{\text{off}}^T + \kappa_{\text{hy}} \lambda)} \quad (13)$$

10

$$S_{Dqss} = \frac{4\pi R N_c A Z_T \kappa_{in} \lambda^3 \kappa_{hy}}{4\pi R \lambda^2 \kappa_{in} (\kappa_{off}^D + \kappa_{hy} \lambda) + \kappa_{off}^D N_c A (\kappa_{off}^T + \kappa_{hy} \lambda)} \quad (14)$$

$$f_{Dqss} = \frac{S_{Dqss}}{S_{qss}} = \frac{\lambda \kappa_{hy}}{\kappa_{off}^D + \kappa_{hy} \lambda} \quad (15)$$

$$p_{qss}(l) = \frac{S_{qss}}{\lambda^2} e^{-l/\lambda} \quad (16)$$

where the parameters at the quasi-steady state are abbreviated by the subscript (qss). It is found from the quasi-steady state, Eqs. (13)-(16), that the steady state ratio of S_D to S (f_{Dqss}) is independent of the radius R and has a theoretical value of $f_{Dqss} = 0.2$ **deduced by** the parameters given in Tab. I. Likewise, we find that $f_{Dqss} \simeq 0.5$ if the hydrolysis rate κ_{hy} increases up to 0.13 s^{-1} . These predicted results are consistent with the experimental results that $\approx 20\%$, or more of the FtsZ monomers within polymers must be hydrolyzed into GDP molecules at the steady state *in vitro*^{2,13}. In addition, the length of filaments within the ring is found to obey with an exponential distribution relevant to the total number of FtsZ monomers in the ring, S_{qss} .

An effective friction between cell wall and fluid environment during cell constrictions is relevant to the local speed, \mathbf{u} , with the assumption of $\mathbf{F}_{fr} = -\tau \mathbf{u}$. Due to the presence of MinCDE proteins in cells, spatial distributions of FtsZ rings are regulated to locate in the middle of cells with a wide range of 25 nm^1 . At the quasi-steady state, the total force in the presence of FtsZ ring that is subsequently controlled **within** a width of 25 nm in the midcell, is approximately zero, that is $\mathbf{F}_{te} + \mathbf{F}_{be} + \mathbf{F}_{ar} + \mathbf{F}_z + \mathbf{F}_{fr} = 0$. But, the force generated by FtsZ rings in other positions is very small, and then can be approximately neglected. Therefore, the total force in absence of the FtsZ ring **is satisfied by** $\mathbf{F}_{te} + \mathbf{F}_{be} + \mathbf{F}_{ar} + \mathbf{F}_{fr} = 0$ at the quasi-steady state. Therefore, the evolution equation of phase field in the presence of FtsZ rings according to Eqs (1)-(10) can be written as

$$\begin{aligned} \frac{\partial \phi}{\partial t} = & -\frac{1}{\tau} \left\{ \kappa (\nabla^2 - \frac{G''}{\epsilon^2}) (\epsilon \nabla^2 \phi - \frac{G'}{\epsilon}) - \gamma (\epsilon \nabla^2 \phi - \frac{G'}{\epsilon}) + M_A (A(\phi) - A_0) |\nabla \phi| \right. \\ & \left. + \frac{B \delta S}{R^3} (R \kappa_T - 1 - \frac{S_D}{S} (\kappa_T - \kappa_D) R) |\nabla \phi| \right\} + \Gamma [\epsilon \nabla^2 \phi - \frac{G'}{\epsilon} + \epsilon c |\nabla \phi|] \end{aligned} \quad (17)$$

and **then** the equation of phase field in absence of FtsZ rings is

$$\frac{\partial \phi}{\partial t} = -\frac{1}{\tau} \left\{ \kappa (\nabla^2 - \frac{G''}{\epsilon^2}) (\epsilon \nabla^2 \phi - \frac{G'}{\epsilon}) - \gamma (\epsilon \nabla^2 \phi - \frac{G'}{\epsilon}) + M_A (A(\phi) - A_0) |\nabla \phi| \right\} + \Gamma [\epsilon \nabla^2 \phi - \frac{G'}{\epsilon} + \epsilon c |\nabla \phi|] \quad (18)$$

The numerical procedure has thoroughly presented in the previous study²⁷ and then is simply given as follows. The fourth order nonlinear partial differential equations (17) and (18) are explicitly solved by an alternating direction implicit scheme and a second order backward differentiation formula. The spaceless partial differential equations, Eqs. (11) and (12), are solved by a forward Euler differential scheme. These space-dependent equations are solved on the simulated box size, $40r_0 \times 20r_0$ with 400×200 grids, where the unit length r_0 is estimated about $0.1 \mu\text{m}$. Therefore, the physical size of the box is about $3 \mu\text{m}$. The simulation time step Δt is 4.0×10^{-5} s. A typical simulation starts with a stationary rod-shaped cell with a surface area $A_0 = 2.78 \mu\text{m}^2$ and an aspect ratio equal to 3.0. The diffusive interface that describes the thickness of cell wall, is chosen as one unit length, $r_0 = 100$ nm. However, the experimental observed thickness of cell wall is observed in the range from 20 to 50 nm^{1,2}. **In the numerical calculations, the interface width is set so small as to cause numerical instability. Therefore, the interface width we chosen is little larger than the experimental value of 20-50 nm.** The dynamic FtsZ ring is assumed to be distributed in the middle of a rod-shaped cell, and has a width of $0.3 r_0$ estimated to 30 nm^2 . The length distribution of FtsZ filaments obeys with the relation of $1/\lambda \cdot e^{-l/\lambda}$, see Eq. (16), where the mean length of FtsZ filaments λ is chosen as 30 monomers. The total number of the monomers within the ring at the initial state is given by $S_{\text{initial}} = \int l p(l, 0) dl$. Therefore, the initial length distribution of filaments within the ring, $p(l, 0)$, is $S_{\text{initial}}/\lambda^2 \cdot e^{-l/\lambda}$. The length distribution and the total number of GDP-bound FtsZ monomers within the ring for the next time step are obtained from the evolution equations (11) and (12). The resulting values of S and S_D are inserted into the evolution equations (17)-(18) of phase field to produce a new shape of a cell. These equations are solved iteratively to obtain the new cell shape, as well as the updated distribution of FtsZ filaments. A steady state is eventually reached when the cell has a stationary shape, and the distribution of FtsZ filaments $p(l, t)$ is independent of the simulation time. The parameters used in the numerical calculations are all comparable to the experimental values^{25,26,28}, as listed in Table I. **However, the two-dimensional simulation parameters are different from those measured three-dimensional values. The parameters listed in Table I have been transformed into two-dimensional parameters by assuming a cell height of $0.1 \mu\text{m}$.** A typical FtsZ rings consisting of the FtsZ monomers has been reported to occupy about 30 % of the total FtsZ monomer in cells. Referring to the set of parameter values given in Table I, we find that the total number of FtsZ monomers within the ring,

S , is about 5500 monomers, which is comparable to the estimated value ranging from 5000 to 15000 FtsZ monomers within the ring in bacterial cells². Then, the total number of FtsZ monomers and GDP-bound FtsZ monomers within the ring, S and S_D , are initially chosen as 5500 and 2200 monomers, respectively.

TABLE I. Model parameters.

	Description	Value	Source
γ	Surface tension	5.0 pN	Simson et al. ³⁷
κ	Bending rigidity	5.0 pN μm^2	Simson et al. ³⁷
τ	Friction coefficient	5×10^2 pN s/ μm^2	Mogilner et al. ³⁸
B	Bending modulus of FtsZ filament	1.2×10^{-2} pN μm^2	Howard et al. ³⁹
ϵ	boundary width	0.1 μm	Shao et al. ²⁶
δ	Size of FtsZ monomer	4 nm	Erickson et al. ¹⁷
Γ	Mobility parameter	0.1 $\mu\text{m}/\text{s}$	Biben et al. ³⁰
κ_T	Intrinsic curvature of GTP-bound FtsZ monomers	0.8 μm^{-1}	Erickson et al. ⁴⁰
κ_D	Intrinsic curvature of GDP-bound FtsZ monomers	80 μm^{-140}	
N_c	Conversion factor	600 $\mu\text{M}^{-1}\mu\text{m}^{-3}$	Allard et al. ²⁵
κ_{in}	Membrane association rate	0.0021 $\mu\text{M}^{-1}\mu\text{m}^{-1}\text{s}^{-1}$	Allard et al. ²⁵
κ_{off}^T	Depolymerization rate of GTP-bound FtsZ monomers	0.1 s^{-1}	Erickson et al. ⁴¹
κ_{off}^D	Depolymerization rate of GDP-bound FtsZ monomers	3.5 s^{-1}	Erickson et al. ⁴¹
κ_{hy}	GTP hydrolysis rate	0.03 s^{-1}	Erickson et al. ⁷
M_A	Area constraint	1.0 pN/ μm^2	Shao et al. ²⁶
λ	Average number of monomers in a filament	30 monomers	
Z_T	Total concentration of FtsZ monomers in cell	13 μM	Erickson et al. ⁴¹

III. RESULTS AND DISCUSSIONS

In our previous study, we have extensively investigated cell morphodynamics during bacterial cytokinesis as functions of different initial states of rod-shaped μm cells and FtsZ rings, such as the aspect ratio, the mean length of FtsZ filaments, the concentration of FtsZ monomers in cells, Z_T , the total number of FtsZ and GDP-bound FtsZ monomers within the ring²⁷. In the

present study, the effect of various kinetic rates, such as the membrane associate rate, κ_{in} , the depolymerization rate, κ_{off}^T and κ_{off}^D , the hydrolysis rates, κ_{hy} , and the intrinsic curvatures, κ_T and κ_D , are studied on cell morphodynamics of cell constrictions in detail.

A. Dynamic process for cell constrictions

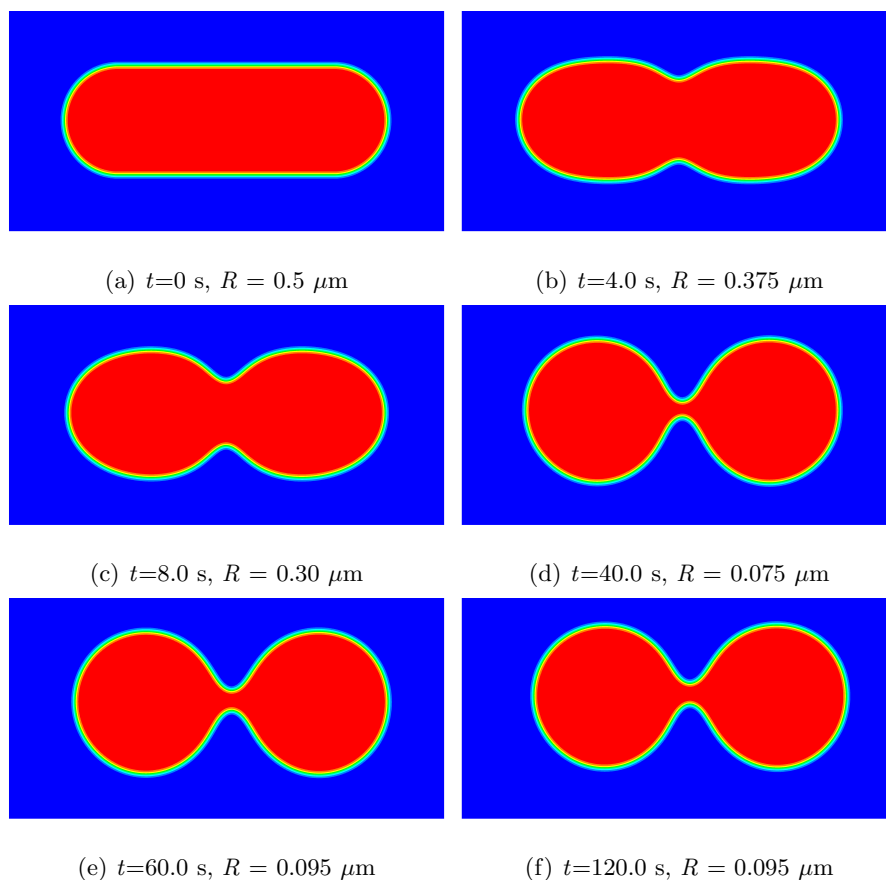


FIG. 2. (color online). Snapshots of the numerical evolution of a cell shape during cell constrictions.

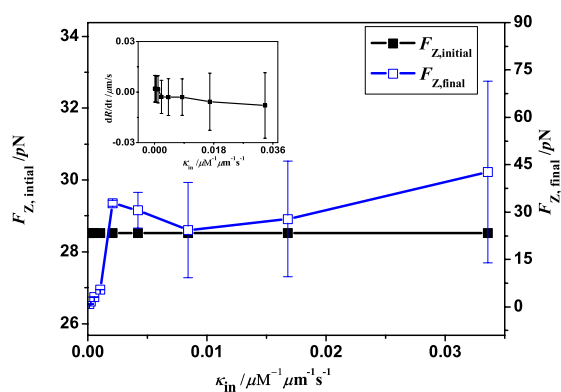
Figure 2 presents an example for the particular set of parameter values given in Table I. During these snapshots, a cell starts with a rod shape at a radius of $0.5 \mu\text{m}$ and has the aspect ratio of 3.0. Along with the dynamical evolution, the cell retracts in the mid-cell down to a radius about $0.095 \mu\text{m}$ at the simulation time $t = 60 \text{ s}$, and then arrives at a steady state. However, the radius at the midcell is found to decrease much less at the simulation time $t = 40 \text{ s}$, and then increases up to $0.095 \mu\text{m}$. The phenomena is attributed that these dynamical FtsZ

rings take much long time to achieve the quasi-steady state. We find that the time for achieving this deformation has the same magnitude with the contraction time of minutes observed in live cells. Likewise, the constriction force is found to be the same magnitude with the previous result that the division can succeed for a wide range of FtsZ-ring force between 8 pN and 80 pN²⁰. In addition, the cell shapes and division time are all comparable to physiologically observed results².

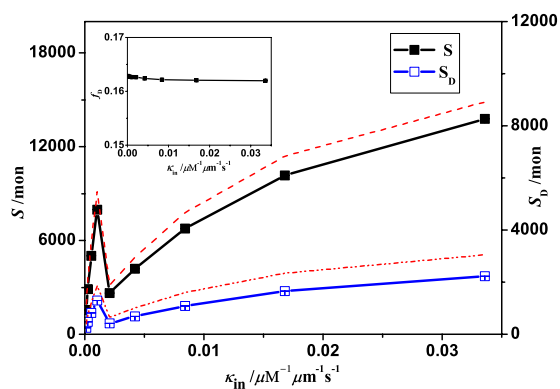
B. The effect of membrane associate rate, κ_{in}

In the *in vitro* experiments, the FtsZ proteins could associate into a membrane binding domain even in the absence of **FtsA proteins which are used for membrane attachments**³⁶. It is estimated in the experiments that the membrane associate rate has a lower bound of $\kappa_{in} = 6 \times 10^{-2} \mu\text{M}^{-1}\mu\text{m}^{-1}\text{s}^{-1}$. **Likewise, the threshold value of κ_{in} is experimentally thought relevant** to the number of bilayers, the membrane bending modulus, and the width of the FtsZ ring²⁵.

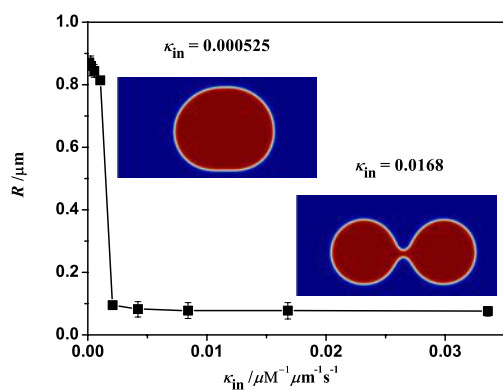
Figure 3 gives cell morphodynamics with respect to the membrane associate rate, κ_{in} with other parameters fixed. The constriction force generated by the FtsZ ring in the initial and steady state, $F_{z,\text{initial}}$ and $F_{z,\text{final}}$, and the contraction rate dR/dt are presented in Fig. 3(a). Inspection of this figure shows that $F_{z,\text{initial}}$ is a constant and independent of κ_{in} , which attributes that the initial states of **the rod-shaped cells and FtsZ rings** are all identical. Whereas, the constriction force at the steady state, $F_{z,\text{final}}$, at first increases rapidly from 0.92 to 32.8 pN with the increase of κ_{in} up to 0.0021, and then $F_{z,\text{final}}$ keeps seriously fluctuations. The contraction rate is larger than zero **until** κ_{in} increases up to 0.0021, because the constriction force exerted on the cell is not high enough to retract the cell wall/membrane, and the rod-shaped cell tends to transform a spherical cell (free energy benefit). This **shape transformation** obeys with the curvature elastic theory. With a further increase of κ_{in} , the cell starts with **the shrinkage rate** of $dR/dt < 0$. Fig. 3(b) gives the number of FtsZ monomers, GDP-bound FtsZ monomers within the ring, S , S_D and the fraction of hydrolyzed monomer in the ring, f_D as a function of the membrane associate rate, κ_{in} . **Similar change trends are** observed for S and S_D that both S and S_D at first increase rapidly as the membrane associate rate, κ_{in} ,



(a)



(b)



(c)

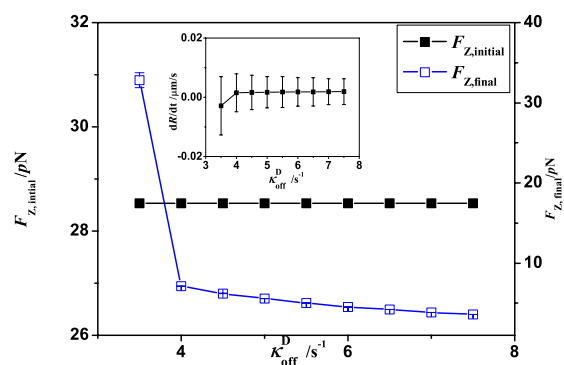
FIG. 3. (color online). The effect of the membrane associate rate on cell constrictions for rod-shaped cells, κ_{in} , (a) constriction forces generated by FtsZ rings at the initial and steady state, and contraction rates in the inset, (b) S , S_D and f_D for FtsZ rings at the steady state, (c) The radius of constrictive rings at the steady state, a cell shape at the steady state with two membrane associate rates given in the inset, respectively.

increases up to 0.0011, then reduce abruptly with a further increase of κ_{in} to 0.0021, and eventually enhance slowly along with the continuous increase of κ_{in} . The changes in S and S_{D} are found to be consistent with the theoretical results given in Eqs. (13) and (14) (red lines). The fraction of hydrolyzed **monomers** in the ring, f_{D} is found close to **an constant** as a function of κ_{in} , which is in good accordance with the theoretical result given in Eq. (15). Fig. 3(c) gives the radius at the midcell, R , with regard to κ_{in} . It is found that the radius, R , decreases along with the increase of κ_{in} up to 0.0021, **and then arrives at 0.08 μm with fluctuations**. Close examination of Fig. 3(b) shows that when κ_{in} is high up to 0.03, S even arrives up to 12000 monomers, but S_{D} increases very slowly. Additionally, we find that with the further increase of κ_{in} up to 0.3, S , S_{D} and R all keep almost unchanged, and even the rod-shaped cell can not divide into two cells. For the change in the membrane associate rate κ_{in} , other parameters, such as the depolymerization rate, the critical concentration and the total concentration of FtsZ monomers in cell, Z_{T} , have to **synthetically** be considered because they would collectively determine the total number of FtsZ monomers and GDP-bound FtsZ monomers within the ring, thereby leading to the transformations of the constriction force and cell shape. **In addition, the change in the radius R at the midcell also has to be considered because it decides the amount of the available binding sites for FtsZ monomers.**

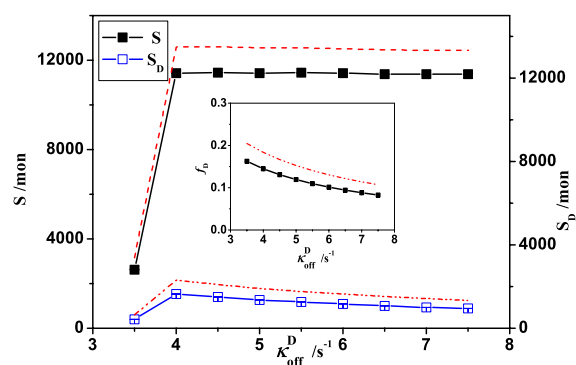
C. The effect of depolymerization rates, κ_{off}^T and κ_{off}^D

In the *in vitro* experiments, an excess of GDP molecules is observed to cause the disassembly of filaments with a half time of 5 s for FtsZ turnover, which is larger than the 9 s half time *in vivo*^{9,15}. Likewise, an excess of GTP molecules is found to possess a comparative longer half time. In addition, different kinetic parameters and **critical concentrations** are experimentally observed for various mutants, such as, FtsZ-L68W and FtsZ-F268C. Therefore, the excess of GDP or GTP molecules, and compound mutants are expected to alter the depolymerization rate of GDP-bound FtsZ or GTP-bound FtsZ monomers at the tip of the filaments^{2,9,10,15}.

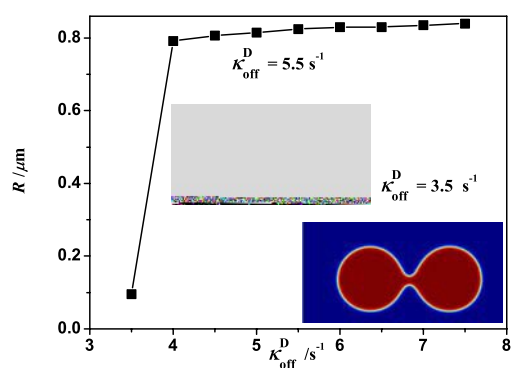
Figure 4 and 5 present the dependences of cell constrictions for rod-shaped cells on the depolymerization rates of GDP-bound and GTP-bound FtsZ monomers at the filament tips, κ_{off}^D and κ_{off}^T , respectively. Figure



(a)

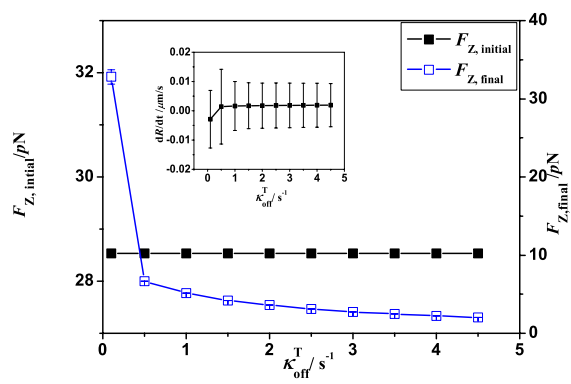


(b)

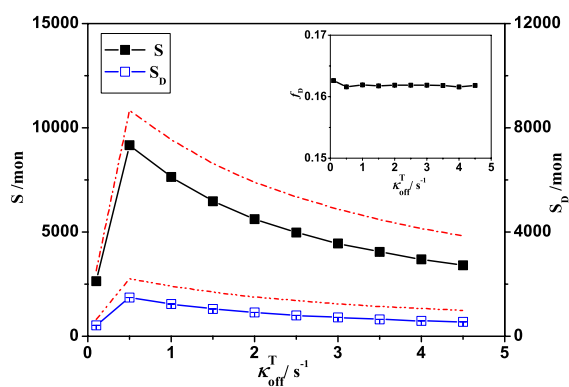


(c)

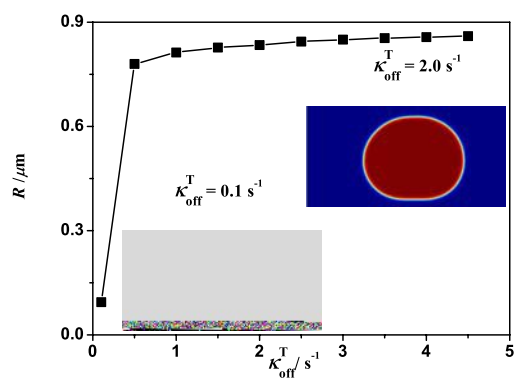
FIG. 4. (color online). The effect of depolymerization rate of GDP-bound FtsZ monomers, $\kappa_{\text{off}}^{\text{D}}$, (a) constriction forces generated by FtsZ rings at the initial and steady state, and contraction rates in the inset, (b) S , S_{D} and f_{D} for FtsZ rings at the steady state, (c) The radius of constrictive rings at the steady state, a cell shape at the initial and steady state given in the inset, respectively.



(a)



(b)



(c)

FIG. 5. (color online). The effect of depolymerization rate of GTP-bound FtsZ monomers, κ_{off}^T , (a) constriction forces generated by FtsZ rings at the initial and steady state, and contraction rates in the inset, (b) S , S_D and f_D for FtsZ rings at the steady state, (c) The radius of constrictive rings at the steady state, a cell shape at the initial and steady state given in the inset, respectively.

4 (a) and 5(a) give the constriction forces exerted on the cell wall at both the initial and steady state upon the changes in the kinetic parameter, $\kappa_{\text{off}}^{\text{D}}$ and $\kappa_{\text{off}}^{\text{T}}$, respectively. Where, the contraction rates, dR/dt , are presented in the insets. Closer examinations in both Fig. 4(a) and 5(a) show that **similar change trends are observed for $F_{\text{Z,initial}}$, $F_{\text{Z,final}}$ and dR/dt** along with the increase of depolymerization rates of both $\kappa_{\text{off}}^{\text{D}}$ and $\kappa_{\text{off}}^{\text{T}}$, where $F_{\text{Z,initial}}$ is found to **be an** constant regardless of the changes in the depolymerization rates, $F_{\text{Z,final}}$ at first decreases rapidly and then slowly upon the increase of both $\kappa_{\text{off}}^{\text{D}}$ and $\kappa_{\text{off}}^{\text{T}}$, and the rod-shaped cell, as expected, contracts rapidly with low depolymerization rates. Due to the same parameters of S , S_{D} and radius of rod-shaped cells in the initial states, the constriction force, $F_{\text{Z,initial}}$, as presented in Eq. (10), is found to be independent of all depolymerization rates. Figure 4 (b) and 5 (b) illustrate the total number of FtsZ monomers and GDP-bound FtsZ monomers within the ring, S and S_{D} , and the fraction of hydrolyzed monomers in the ring, f_{D} , at steady state upon the changes in $\kappa_{\text{off}}^{\text{D}}$ and $\kappa_{\text{off}}^{\text{T}}$, respectively. The red lines presented in Fig. 4 (b) and 5 (b) are the theoretical results derived from Eqs. (13)-(15). It is found that S at first increases and then maintains fluctuations upon the increase of $\kappa_{\text{off}}^{\text{D}}$, while S at first increases up to the radius of midcell, R , close to 0.7, and then decreases gradually upon the further increase of $\kappa_{\text{off}}^{\text{T}}$. The difference between the dependences of S on $\kappa_{\text{off}}^{\text{D}}$ and $\kappa_{\text{off}}^{\text{T}}$ is possible to be attributed that the GDP-bound FtsZ monomer within the ring originates from the hydrolysis of GTP-bound FtsZ monomer, as well as the fraction of the hydrolyzed monomers is theoretically less than 20%, thereby giving that the change in the depolymerization rate of GTP-bound FtsZ monomer would seriously influence the number of FtsZ monomers within the ring. However, **the same trend is observed for S_{D}** as functions of the depolymerization rates that S_{D} at first increases up to the radius of midcell close to one spherical cell, and then decreases gradually with a further increase of the depolymerization rate whether $\kappa_{\text{off}}^{\text{T}}$ or $\kappa_{\text{off}}^{\text{D}}$. In the insets of Fig. 4 (b) and 5 (b), the fraction of the hydrolyzed monomers in the ring, f_{D} descends upon the increase of $\kappa_{\text{off}}^{\text{D}}$, but **remains an constant** along with the increase of $\kappa_{\text{off}}^{\text{T}}$. The result is confirmed in Eq. (15) that f_{Dqss} is independent of $\kappa_{\text{off}}^{\text{T}}$, but is expected to respond to $\kappa_{\text{off}}^{\text{D}}$. Likewise, it is shown in both Fig.4 (b) and 5 (b) that S and S_{D} obtained from the calculations are in good consistent with the theoretical lines (red). Figure 4 (c) and 5 (c) give the radius of midcell, R , at the steady state as functions of the depolymerization rates. It is found in both Fig. 4 (c) and 5(c) that the rod-shaped cell starts with contract when $\kappa_{\text{off}}^{\text{D}}$ decreases from 7.8 s^{-1} to 3.5 s^{-1} , whereas the rod-shaped cell is also able to contract when $\kappa_{\text{off}}^{\text{T}}$ shifts from 4.8 s^{-1} down to 0.5 s^{-1} . As

a whole, the rod-shaped cell with low depolymerization rate would enhance the number of FtsZ monomers within the ring, thereby leading to the increased constriction force and seriously cell constriction.

D. The effect of hydrolysis rates, κ_{hy}

Assembly dynamics of FtsZ monomers is regulated by the binding, hydrolysis, and exchange of GTP molecules. The mutant FtsZ84 hydrolyzes GTP molecules at a rate one tenth that of wild-type cells^{7,13}. *In vitro*, this reduced GTPase activity is observed to increase the fraction of **FtsZ monomers within** the ring even up to 65 %. Likewise, a half time for the mutant FtsZ ring is found high up to 30 s by FRAP analysis, giving that a slow monomer turnover compares with the wild-type half time of 9 s¹³. In addition, the exchange of FtsZ monomers can be strongly reduced by the slowly hydrolyzable nucleotide GMPCMP. The average time for a FtsZ monomer resided in the ring, τ_{re} , can be estimated by the relation of $\tau_{\text{re}} = 1/\kappa_{\text{hy}} + \lambda/2\kappa_{\text{off}}^D$. Therefore, **the half life of FtsZ monomers within** the ring is observed to increase with such **a reduction** in the hydrolysis rate or slowly disassembly of GDP-bound FtsZ monomers.

Figure 6 illustrates **cell constrictions** of rod-shaped cells with respect to GTP hydrolysis rate, κ_{hy} , with all other parameters unchanged. Due to all other parameters unchanged, the constriction force as shown in Fig. 6(a) is still found **close to an constant** irrespective of the alteration in the hydrolysis rate, κ_{hy} . The constriction force generated by FtsZ ring at the steady state at first shows a slowly enhancement upon the increase of κ_{hy} . With a further increase of κ_{hy} , the constriction force $F_{\text{Z,final}}$ increases suddenly along with the rapidly decrease of radius at the midcell, R . Fig. 6(b) presents S , S_{D} and f_{D} in response to the hydrolysis rate κ_{hy} . It is found that the total number of FtsZ monomers within the ring, S , decreases slowly when the hydrolysis rate increases from 0.001 s^{-1} to 0.025 s^{-1} . Then, with a further increase in the hydrolysis rate, the radius at the midcell starts seriously with the contraction, as well as S rapidly decreases. The result agrees well with the *in vivo* phenomena that the reduced GTPase activity would increase the fraction of FtsZ monomers within the ring. However, the total number of GDP-bound FtsZ monomers within the ring, S_{D} , at first increases along with the increase of κ_{hy} , and then decreases with further increase of κ_{hy} at the beginning of cell contractiles. In the inset of Fig. 6(b), the fraction of hydrolyzed monomers in the ring,

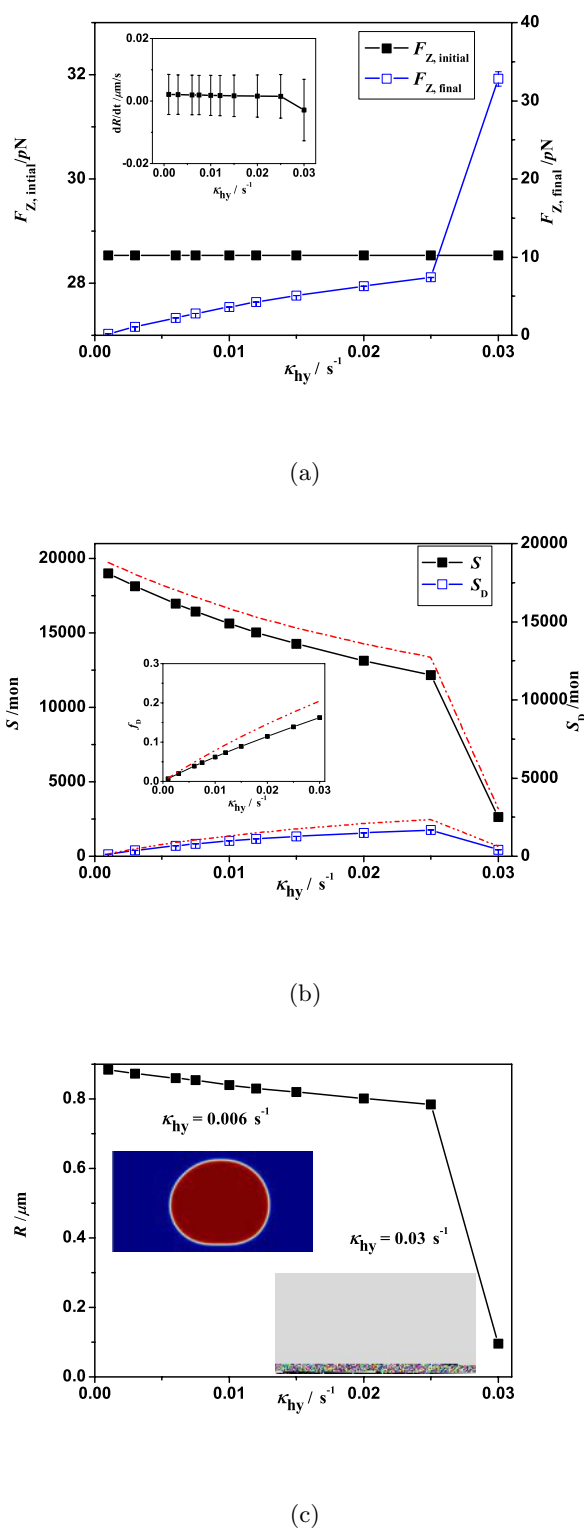


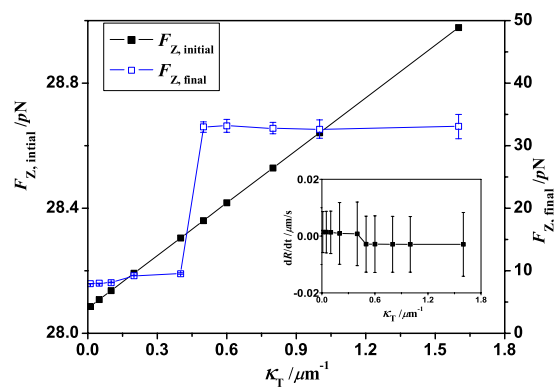
FIG. 6. (color online). The effect of hydrolysis rate, κ_{hy} , (a) constriction forces generated by FtsZ rings at the initial and steady state, and contraction rates in the inset, (b) S , S_D and f_D for FtsZ rings at the steady state, the red lines are obtained from the theoretical values, Eqs. (13)-(15), (c) The radius of constrictive rings at the steady state, a cell shape at the steady state given in the inset.

f_D , **is found to increase** monotonously as a function of κ_{hy} . Likewise, the radius at the midcell reduces along with such an increase in κ_{hy} , as shown in Fig. 6(c). Therefore, with such an enhancement in κ_{hy} , it seems that the fraction of the hydrolyzed monomers in the ring, f_D , increases, and then the constriction force would gradually increase up to the force required to divide the cell, thereby giving the reduction of the radius at the midcell.

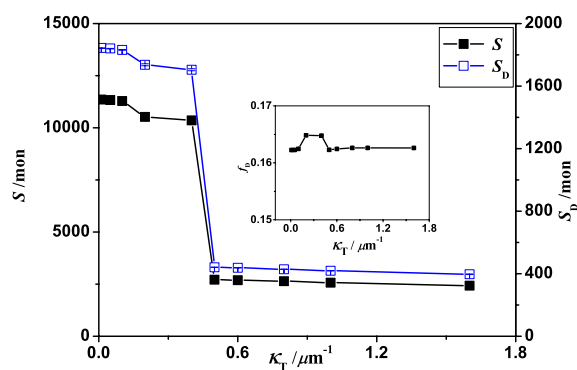
E. The effect of intrinsic curvatures, κ_T and κ_D

FtsZ is experimentally observed to contain a GTP hydrolysis cycle, allowing it to take at least two main preferred states^{6,16}. When bound to GTP, filaments prefer to be straight, but upon hydrolysis, the preferred conformation is curved with a radius of curvature about 12-13 nm. It is noted that the absolute minimal radius for which the constriction mechanism can generate an inward force, is the intrinsic radius of curvature, such as $1/\kappa_D \simeq 12.5$ nm and $1/\kappa_T \simeq \infty$ ²⁵. Therefore, κ_T is well known to be far less than κ_D .

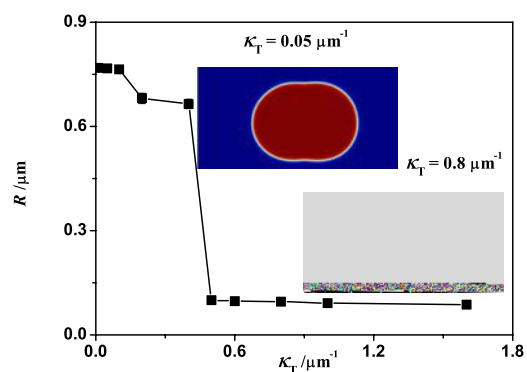
Figure 7 and 8 present the dependences of cell morphodynamics on the intrinsic curvatures, κ_T and κ_D , with all other parameters fixed. It is seen from both Fig. 7 (a) and 8 (a) that the constriction forces at the initial state increase linearly along with the intrinsic curvatures κ_T and κ_D , which are in well accordance with the trend given in Eq. (10). However, as shown in Fig. 7(a), the constriction force at the steady state, $F_{z,final}$, increases slowly with an increase of κ_T up to $0.4 \mu m^{-1}$, but jumps abruptly to a high level with κ_T close to $0.45 \mu m^{-1}$, together with R shrinking down to $0.1 \mu m$. Then with the further increase of κ_T up to $1.6 \mu m^{-1}$, $F_{z,final}$ grows very slowly. Further increasing κ_T up to $2.4 \mu m^{-1}$, the rod-shaped cell completely divides into two parts at the steady state. As shown in Fig. 8(a), **a different change** is observed in the dependence of $F_{z,final}$ on κ_D that $F_{z,final}$ increases gradually along with the continuous increase of κ_D from $5 \mu m^{-1}$ to $70 \mu m^{-1}$, **along with the increase of** the shrinkage of R down to $0.1 \mu m$, and then $F_{z,final}$ increases rapidly up to 32.82 ± 0.93 pN (close to the force required to cell constriction). Fig. 7 (b) and 8 (b) present the dependences of S , S_D and f_D on the intrinsic curvatures, κ_T and κ_D . Along with increase of the intrinsic curvatures, **both** S and S_D at first decline gradually, and then suddenly reduce, as well as R shrinks close to $0.1 \mu m$ (see Fig. 7 (c) and 8 (c)). With the further increase of the intrinsic curvatures,



(a)



(b)



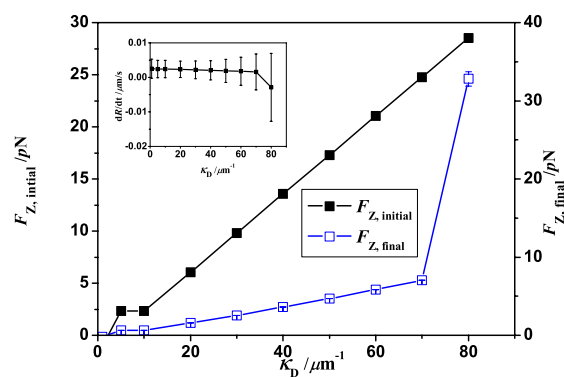
(c)

FIG. 7. (color online). The effect of intrinsic curvature, κ_T , (a) constriction forces generated by FtsZ rings at the initial and steady state, and contraction rates in the inset, (b) S , S_D and f_D for FtsZ rings at the steady state, (c) The radius of constriction rings at the steady state, a cell shape at the steady state given in the inset.

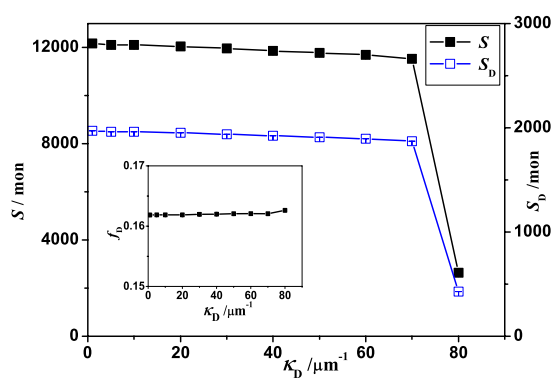
both S and S_D decrease slowly till to cell division. **However**, f_D is found to be independent of the intrinsic curvatures, **which are identical to the theoretical derivation of** Eq. (15).

F. Phase diagram

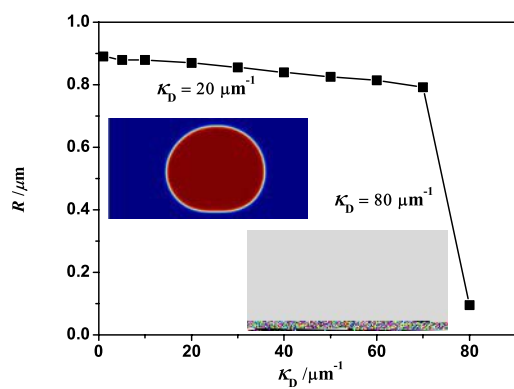
Phase diagram is presented in Fig. 9 that the state of rod-shaped cells **at the steady state is described** as functions of the membrane associate rate constant, κ_{in} , and the depolymerization rate of GDP-bound FtsZ monomers, κ_{off}^D , where division and undivision are used to distinguish the final state of cells. It is found that when the depolymerization rate of GDP-bound FtsZ monomers, κ_{off}^D , is larger than 4.2 s^{-1} , **rod-shaped cells can not completely realize cell divisions irrespective of the membrane associate rate. Referring to Eq. 11, the associate rate of FtsZ monomers to the membrane is related to the binding sites with respect to the radius at the midcell R and the membrane associate rate constant κ_{in} , where R at the steady state is found to decrease with the increase of κ_{in} .** We also can turn to the effect of the depolymerization rate of GDP-bound FtsZ monomers, κ_{off}^D on cell morphodynamics, see Sec. III C. With the increase of κ_{off}^D up to a certain value, the number of FtsZ monomers within the ring keeps almost unchanged. That is, one monomer associates to the ring underlying the cell membrane, and then another monomer will detach from the ring right now to the cytoplasmic pool, thereby leading to the number of monomers within the ring unchanged. Inspection of Fig. 9 shows that the final state of rod-shaped cell is mainly determined by the depolymerization rate of GDP-bound FtsZ monomers. However, Figure 3 presents that **the radius at the midcell at the steady state** will contract with the increase of the membrane associate rate at $\kappa_{off}^D = 3.5 \text{ s}^{-1}$. Similarly, with the further increase of κ_{in} , **as well as the reduced radius at the midcell**, the original cell can not divide into two parts **completely**. The main reason is that at this κ_{off}^D , the number of **GDP-bound FtsZ monomers** within the ring which makes the main contribution to the constriction force, can not generate enough force to **cell divisions**, although the number of **FtsZ monomers** within the ring, S , can to a certain extent increase as a function of κ_{in} . Therefore, cell division is determined by the collective contributions of various kinetic rates.



(a)



(b)



(c)

FIG. 8. (color online). The effect of intrinsic curvature, κ_D , (a) constriction forces generated by FtsZ rings at the initial and steady state, and contraction rates in the inset, (b) S , S_D and f_D for FtsZ rings at the steady state, (c) The radius of constriction rings at the steady state, a cell shape at the steady state given in the inset.

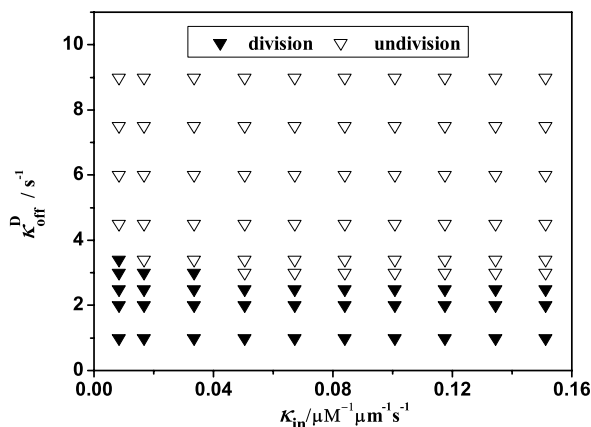


FIG. 9. (color online). Phase diagram as a function of the membrane associate rate of short FtsZ filaments/ free FtsZ monomers, κ_{in} , and the depolymerization rate of GDP-bound FtsZ monomers, κ_{off}^D .

IV. SUMMARY AND OUTLOOK

A new theoretical framework by a combination of phase field model for cells and a kinetics description for FtsZ ring maintenance has been developed to investigate bacterial cytokinesis in our previous study²⁷. A typical dynamic process of **cell constrictions with reasonable parameters**, comparable to the experimental values, has been studied. It is found that a rod-shaped cell would start to shrink at the midcell when the constriction force is above 28 pN that is the least force required to cell constrictions. The force required to cell constrictions has the same magnitude with the previous report²⁰. In addition to the critical force, the obtained cell shapes and division times are all comparable to physiologically observed results². At the same time, cell morphodynamics during cell constrictions have been studied as functions of different initial states of rod-shaped cells and FtsZ rings, such as the aspect ratio, the mean length of FtsZ filaments, the concentration of FtsZ monomers in cells, Z_T , the total number of FtsZ and GDP-bound FtsZ monomers within the ring. The effects of various kinetic rates, such as the membrane associate rate, κ_{in} , the depolymerization rate, κ_{off}^T and κ_{off}^D , the hydrolysis rate, κ_{hy} , and the intrinsic curvatures, κ_T and κ_D , are studied on cell morphodynamics of cell **constrictions** in the present study.

Since all initial states of the rod-shaped cells are identical, the constriction forces generated by FtsZ rings

at the initial state are found to independent of various kinetic rates. The radius at the midcell, R , is observed to reduce along with such an increase of κ_{in} , κ_{hy} , the intrinsic curvatures, κ_{T} and κ_{D} . Such an increase in κ_{in} and κ_{hy} would lead to the enhancement of the number of FtsZ monomers or GDP-bound FtsZ monomers within the ring, **eventually giving rise to the increase of the constriction force**. The increase of the intrinsic curvatures, κ_{T} and κ_{D} , would enhance the mechanical energy exerted on the cell wall/membrane, as well as the constriction force. Conversely, the increase of the depolymerization rates, $\kappa_{\text{off}}^{\text{T}}$ and $\kappa_{\text{off}}^{\text{D}}$, causes such a reduction of the constriction force, thereby leading to an expansion of the rod-shaped cell. **It is found that with suitable parameters, the radius at the midcell is to be abruptly changed, together with the rapid transformation of the constriction force, S and S_{D} at the steady state. When the force generated by FtsZ rings is above the critical force, the radius at the midcell starts to retract. Likewise, the associate binding rate of FtsZ monomers or short filaments would be changed due to the reduce of binding sites, together with the change for the quasi-steady state of FtsZ ring maintenance. Therefore, the radius at the midcell would abruptly shrink to small values.** In addition, the number of FtsZ monomers and GDP-bound FtsZ monomers within the ring, S and S_{D} , are found to alter non-monotonously as functions of the membrane associate rate, κ_{in} , the depolymerization rate, $\kappa_{\text{off}}^{\text{T}}$ and $\kappa_{\text{off}}^{\text{D}}$, and the hydrolysis rate, κ_{hy} . In addition, the quasi-steady state for the dynamic turnover of FtsZ rings, including S , S_{D} and f_{D} , are in good accordance with the theoretical results derived from Eqs. (13)-(15).

In order to explicitly elucidate the relation of cell constrictions and some kinetic rate parameters, morphological phase diagram is presented as functions of the membrane associate rate, κ_{in} , and the depolymerization rate of GDP-bound FtsZ monomers, $\kappa_{\text{off}}^{\text{D}}$. It is found that the final states of cells are mostly determined by the depolymerization rate of GDP-bound FtsZ monomers, $\kappa_{\text{off}}^{\text{D}}$, but have to take the effect of other kinetic rates into account.

The basic theoretical framework has been successfully applied to study bacterial cytokinesis, which has evident advantage to couple FtsZ ring with cell shape. A more detailed discussion relevant to various kinetic rates within the FtsZ ring has been presented in the present work. **As we known, the incorporation of regulatory proteins would affect the kinetic rates within the FtsZ ring. The result presented**

here would provide the theoretical basis to control bacterial cytokinesis. Likewise, the quasi-steady states of FtsZ dynamical rings are mainly focused in the present study. The typical parameters used in Table I are satisfied with the contraction of rod-shaped cells at the midcell, but the rod-shaped cells can not divide completely. It is also of great interests to study the phenomena of the rod-shaped cells dividing into two complete parts in futures studies. Additionally, it is very important to develop other space dependent theoretical framework aimed to study the spatial structure and dynamic turnover of FtsZ rings.

ACKNOWLEDGMENTS

The financial supports of this work are provided by the Fundamental Research Funds for the Central Universities, the National Natural Science Foundation of China (Grant No. 21274038, 21403200).

-
- ¹ J. Lutkenhaus *Annu. Rev. Biochem* **76**, 539-562 (2007).
 - ² H. P. Erichson, D. E. Anderson, M. Osawa *Microbio. Mol. Rev.* **74**, 504 (2010).
 - ³ P. De. Boer, R. Crossley, L. Rothfield *Nature* **359**, 254 (1992).
 - ⁴ D. RayChaudhuri, J. T. Park, *Nature* **359**, 251 (1992).
 - ⁵ Mukherjee A, Lutkenhaus *J EMBO J.* **17**, 462-468 (1998).
 - ⁶ M. Osawa, D. E. Anderson, H. P. Erickson *Science* **320** 792 (2008).
 - ⁷ J. Stricker, P. Maddox, E. D. Salmon, H. P. Erickson, *Proc. Natl. Acad. Sci. USA* **99**, 3171 (2002).
 - ⁸ M. Osawa, H. P. Erickson, *EMBO J.* **28**, 3476-3484 (2009).
 - ⁹ A. Dajkovic, G. Lan, S. Sun, D. Wirtz, J. Lutkenhaus *Curr. Biol.* **18**, 235 (2008).
 - ¹⁰ K. H. Huang, J. D. Heredia, A. Janakiraman *J. Bacteriology* **195**, 1859 (2013).
 - ¹¹ Z. Hu, A. Mukherjee, J. Lutkenhaus *Proc. Natl. Acad. Sci. USA* **96**, 14819 (1999).
 - ¹² D. J. Scheffers *FEBS Lett* **582**, 2601 (2008).
 - ¹³ Anderson D, Gueiros-Filho F., Erickson H J. *Bacteriol* **186**, 5775 (2004).
 - ¹⁴ P. A. Levin, I. G. Kurtser, A. D. Grossman *Proc. Natl. Acad. Sci. USA* **96**, 9642 (1999).

- ¹⁵ N. L. Elsen, J. Lu, K. J. Lumb, J. Am. Chem. Soc. **134**, 12342 (2012).
- ¹⁶ L. Romberg, M. Simon, H. Erickson, J. Biol. Chem. **276**, 11743 (2001).
- ¹⁷ H. Erickson, D. Taylor, K. A. Taylor, Proc. Natl. Acad. Sci. USA **93**, 519 (1996).
- ¹⁸ J. M. Gonzalez, M. Jimenez, J. Mingorance, J. Biol. Chem. **278**, 37664 (2003).
- ¹⁹ J. Hsin, A. Gopinathan, K. C. Huang Proc. Natl. Acad. Sci USA **109**, 9432 (2012).
- ²⁰ G. Lan, C. Wolgemuth, S. Sun Proc. Natl. Acad. Sci USA **104**, 16110 (2007).
- ²¹ H. P. Erichson Proc. Natl. Acad. Sci. USA **106**, 9238 (2009).
- ²² B. Ghosh, A. Sain Phys. Rev. Lett. **101**, 178101 (2008).
- ²³ G. H. Lan, B. R. Daniels, T. M. Dobrowsky, D. Wirtz, S. X. Sun Proc. Natl. Acad. Sci. USA **106**, 121 (2009).
- ²⁴ G. H. Lan, A. Dajkovic, S. X. Sun Biophys. J. **95**, 4045 (2008).
- ²⁵ J. F. Allard, E. N. Cytrynbaum Proc. Natl. Acad. Sci. USA **106**, 145 (2009).
- ²⁶ D. Y. Shao, W. J. Rappel, H. Levin Phys. Rev. Lett. **105**, 18104 (2010).
- ²⁷ Z. Liu, K. K. Guo RSC Advances **4** 56665 (2014).
- ²⁸ Z. Liu, K. K. Guo Acta Chim. Sinica **17**, 1183 (2013).
- ²⁹ R. Folch, J. Casademunt, A. H. Machado, Phys. Rev. E. **60**, 1724 (1999).
- ³⁰ T. Biben, K. Kassner, C. Misbah, Phys. Rev. E. **72**, 041921 (2005).
- ³¹ J. S. Lowengrub, A. Ratz, A. Voigt, Phys. Rev. E. **79**, 031926 (2009).
- ³² Q. Du, C. Liu, X. Wang, J. Comput. Phys. **212**, 757 (2006).
- ³³ K. Keren, Nature **453**, 475 (2008).
- ³⁴ L. Landau, L. Pitaevskii, E. Lifshitz, Theory of Elasticity, Pergamon Press (1986).
- ³⁵ K. K. Guo, J. Shillcock, R. Lipowsky, J. Chem. Phys. **133**, 155105, (2010).
- ³⁶ X. L. Ma, D. W. Ehrhardt, W. Margolin Proc. Natl. Acad. Sci. USA **93**, 12998 (1996).
- ³⁷ R. Simson et. al. Biophys. J. **74**, 514(1998).
- ³⁸ K. Larripa, A. Mogilner Physica **372A**, 113(2006).
- ³⁹ B. Mickey, J. Howard J. Cell Biol. **130**, 909(1995).
- ⁴⁰ C. Lu, M. Reedy, H. Erichson J. Bacteriol. **182**, 164 (2000).
- ⁴¹ Y. Chen, H. Erichson J. Biol. Chem. **280**,22549(2005).